Journal of Materials Chemistry

www.rsc.org/materials

Volume 17 | Number 30 | 14 August 2007 | Pages 3053–3272

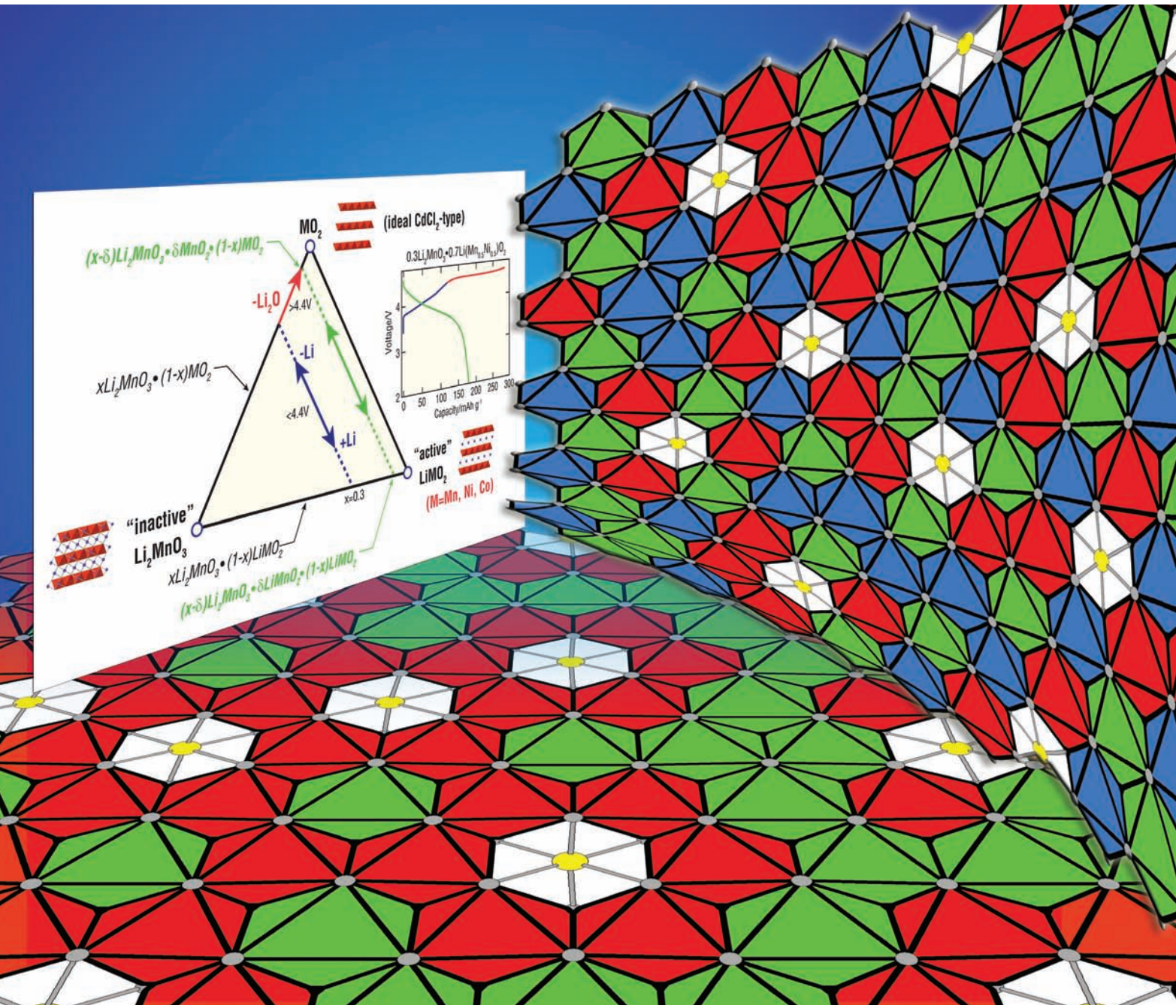

ISSN 0959-9428

Theme Issue: New Energy Materials

FEATURE ARTICLE
Michael M. Thackeray *et al.*
Li_2MnO_3-stabilized $LiMO_2$ (M = Mn, Ni, Co) electrodes for lithium-ion batteries

Chemical Technology

In this issue...

0959-9428(2007)17:30;1-0

RSC Publishing

Li_2MnO_3-stabilized $LiMO_2$ (M = Mn, Ni, Co) electrodes for lithium-ion batteries†

Michael M. Thackeray,*[a] Sun-Ho Kang,[a] Christopher S. Johnson,[a] John T. Vaughey,[a] Roy Benedek[a] and S. A. Hackney[b]

Received 16th February 2007, Accepted 29th March 2007
First published as an Advance Article on the web 20th April 2007
DOI: 10.1039/b702425h

A strategy used to design high capacity (>200 mAh g^{-1}), Li_2MnO_3-stabilized $LiMO_2$ (M = Mn, Ni, Co) electrodes for lithium-ion batteries is discussed. The advantages of the Li_2MnO_3 component and its influence on the structural stability and electrochemical properties of these layered $xLi_2MnO_3{\cdot}(1-x)LiMO_2$ electrodes are highlighted. Structural, chemical, electrochemical and thermal properties of $xLi_2MnO_3{\cdot}(1-x)LiMO_2$ electrodes are considered in the context of other commercially exploited electrode systems, such as $LiCoO_2$, $LiNi_{0.8}Co_{0.15}Al_{0.05}O_2$, $Li_{1+x}Mn_{2-x}O_4$ and $LiFePO_4$.

1. Introduction

The introduction of non-aqueous rechargeable *lithium-ion* batteries in the 1990s to power portable electronic devices created a revolution in battery technology and a marked swing away from the relatively low-voltage, water-based systems such as nickel–cadmium and nickel–metal hydride batteries and high-temperature systems.[1] The first commercial lithium-ion battery, introduced into the market by Sony Corporation in 1991, was based on a $Li_xC_6/Li_{1-x}CoO_2$ couple. During cell operation between 4.2–3.0 V, lithium ions are transported electrochemically between the two electrodes, with concomitant oxidation and reduction of the Li_xC_6 anode[2,3] and $Li_{1-x}CoO_2$ cathode,[4] respectively, during discharge and *vice versa* during charge. The surface reactivity and instability of delithiated $Li_{1-x}CoO_2$ limit the practical capacity of $LiCoO_2$ electrodes to approximately 140 mAh g^{-1}, which corresponds to $x \approx 0.5$, *i.e.*, ~50% of its theoretical value (273 mAh g^{-1}). These limitations and the relatively high cost of cobalt, have led to enormous efforts since 1991 to find alternative cathode materials to $LiCoO_2$ that provide lithium-ion cells with superior capacity, energy, safety and cycle life.

Several alternative cathode materials to $LiCoO_2$ have been exploited by the lithium battery industry over the past decade; they include compositional variations of the layered $LiCoO_2$ structure, such as $LiNi_{0.80}Co_{0.15}Al_{0.05}O_2$,[5] spinel electrodes derived from $LiMn_2O_4$,[6,7] such as lithium-rich compounds in the $Li_{1+x}Mn_{2-x}O_4$ system,[8] and $LiFePO_4$, which has an olivine-type structure.[9,10] Although $LiNi_{0.80}Co_{0.15}Al_{0.05}O_2$ provides a slightly higher practical capacity (160–180 mAh g^{-1}) than $LiCoO_2$, its thermal instability on

[a]*Battery Technology Department, Chemical Engineering Division, Argonne National Laboratory, Argonne, Illinois 60439, USA*
[b]*Department of Metallurgical and Materials Engineering, Michigan Technological University, Houghton, Michigan 49931, USA*
† This paper is part of a *Journal of Materials Chemistry* theme issue on New Energy Materials. Guest editor: M. Saiful Islam.

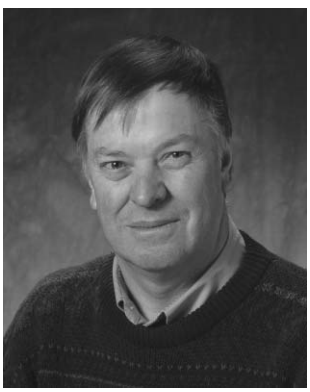

Michael Thackeray

Michael Thackeray received his B.S. (1970), M.S. (1973) and Ph.D. (1977) degrees in Chemistry from the University of Cape Town, South Africa and studied as a postdoctoral fellow with Professor John B. Goodenough at Oxford University, UK. After spending twenty years at the Council for Scientific and Industrial Research (CSIR), Pretoria, South Africa (1973–1994) on battery-related research, he moved to the United States where he is currently an Argonne Distinguished Fellow and Group Leader at Argonne National Laboratory outside Chicago. His primary research interest is determining the structure–electrochemical properties of solid electrolyte and electrode materials for electrochemical applications.

Sun-Ho Kang

Sun-Ho Kang received his B.S. (1992), M.S. (1994), and Ph.D. (1998) in Materials Science and Engineering from Seoul National University, South Korea. After studying as a postdoctoral fellow with Professor John B. Goodenough at the University of Texas at Austin (1999–2000), he joined the Chemical Engineering Division at Argonne National Laboratory. His primary research interests include synthesis, electrochemical and transport properties, and structure–property relationships of electrode materials for energy storage and conversion systems.

delithiation compromises the safety of lithium-ion cells.[11] On the other hand, spinel $LiMn_2O_4$ and olivine $LiFePO_4$ electrodes are significantly more stable to lithium extraction than the layered Co- and Ni-based electrodes, both structurally and thermally, but they deliver relatively low practical capacities above 3 V in a lithium cell, typically 100–120 mAh g^{-1} at moderate current rates. (The theoretical capacities of $Li_{1-x}Mn_2O_4$ and $Li_{1-x}FePO_4$ for the complete extraction of lithium (x = 1) are 148 and 170 mAh g^{-1}, respectively.) It was clear by the end of the 1990s that new strategies would have to be developed to design alternative high potential cathode materials (>3 V *vs.* Li^0) with superior capacities to standard $LiCoO_2$-, $LiMn_2O_4$- and $LiFePO_4$-type electrodes without compromising the structural stability or rate capability of the electrodes or the cycle life of the cells. In this Feature Article, the strategy that was adopted at Argonne National Laboratory to develop a family of high capacity, Li_2MnO_3-stabilized $LiMO_2$ (M = Mn, Ni, Co) electrodes for lithium-ion batteries is highlighted; progress made at Argonne and by others in advancing this class of electrode materials is briefly reviewed.

2. Strategy

Insertion electrodes for lithium-ion electrochemical cells need to have stable structures over a wide compositional range so that as much lithium as possible can be inserted and extracted during repeated discharge and charge to maximize cell capacity, energy and cycle life. Furthermore, the host structure must have an interstitial space that provides energetically favorable pathways for fast lithium-ion transport, *i.e.*, a high power capability. A common procedure used to stabilize metal oxide electrode structures is cation or anion substitution. For example, 1) in $LiNi_{0.80}Co_{0.15}Al_{0.05}O_2$, Al^{3+} ions are used to provide greater binding energy to the oxygen sheets of the layered structure on delithiation, 2) Li^+ substitution for Mn^{3+} in $LiMn_2O_4$, *i.e.*, $Li_{1+x}Mn_{2-x}O_4$, increases the relative Mn^{4+}-ion concentration in the spinel structure which suppresses the manganese solubility in lithium-ion battery electrolytes,[8,12] and 3) fluorine substitution for oxygen in spinel[13,14] and layered[15,16] electrodes, particularly at the particle surface, provides enhanced cycling stability. An alternative approach to impart structural stability and improve the electrochemical

Christopher S. Johnson

Christopher S. Johnson holds a B.S. in Chemistry from the University of North Carolina at Chapel Hill (1987) and a Ph.D. in Inorganic Chemistry from Northwestern University (1992). He is currently a staff chemist in the Chemical Engineering Division at Argonne National Laboratory. Dr Johnson's professional interests include the development of new synthetic methods and the use of spectroscopy and electrochemistry to solve problems in materials science. He conducts applied research in lithium batteries, and basic research in studies of ionic transport and mechanisms, electron transfer processes, intercalation structures and phase diagrams of materials.

John Vaughey

John Vaughey received his B.S. in Chemistry from Worcester Polytechnic Institute (1987) and his Ph.D. in Inorganic Chemistry from Northwestern University (1992) under the direction of Professor Ken Poeppelmeier. Since completing postdoctoral positions with Professor Allan Jacobson at the University of Houston and Professor John D. Corbett at Iowa State University/Ames Laboratory, he has worked in the Chemical Engineering Division of Argonne National Laboratory since 1997. His primary research interests include structure–property relationships in metal oxides, primary and secondary lithium-ion battery materials.

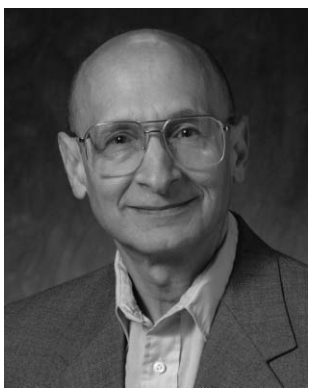

Roy Benedek

Roy Benedek received B.S. and M.Eng. degrees in Engineering Physics from Cornell University, and a Ph.D. in Theoretical Solid State Physics from Brown University. He was a postdoctoral research associate at Cornell University before joining the Materials Science Division at Argonne National Laboratory. He is presently a Special Term Appointee with the Battery Materials Group in the Chemical Engineering Division at Argonne. His primary research interest is the simulation of structural and electronic properties of materials.

Stephen Hackney

Stephen Hackney received his B.S. in Chemistry from James Madison University (1980), and M.S. (1982) and Ph.D. (1985) degrees in Materials Science from the University of Virginia. In 1985–86, he spent 18 months as a postdoctoral fellow with Professor John W. Cahn at NIST. He spent the following 20 years as a faculty member in the Department of Materials Science and Engineering at Michigan Technological University. His primary research interests have been materials characterization and crystallographic phase transformations, with a focus on electrode materials for electrochemical applications.

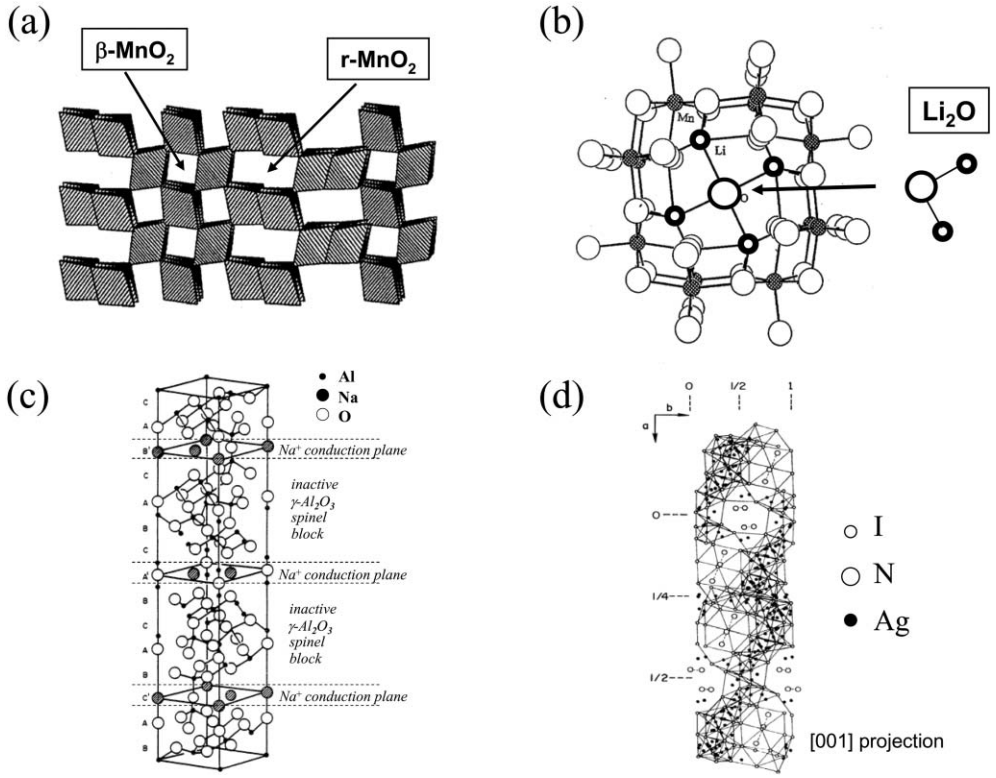

Fig. 1 Schematic illustrations of the structures of a) γ-MnO_2 [after ref. 17]; b) Li_2O-stabilized α-MnO_2 [after ref. 19]; c) β''-alumina, $Na_2O{\cdot}5.3Al_2O_3$ after [ref. 20] and d) $44AgI{\cdot}3(C_{11}H_{22}N_3)I_3$ [after ref. 22]. Figures reproduced from the respective references, Fig 1a, 1b and 1c with permission from Elsevier and Fig. 1d from the International Union of Crystallography (http://journals.iucr.org/).

properties of solid electrode and solid electrolyte materials is to use structural units rather than cation or anion substituents. For example, in the family of MnO_2 electrodes, γ-MnO_2, which is used in 3 V lithium cells, has a composite structure containing unidimensional (2 × 1) ramsdellite-type tunnels (designated r-MnO_2 in Fig. 1a) that can accommodate lithium, and narrow (1 × 1) rutile-like tunnels (designated β-MnO_2 in Fig. 1a) that are essentially impervious to lithium and impart stability to the overall structure.[17] Another example of a 3 V electrode is α-MnO_2 with a hollandite-type structure that provides enhanced electrochemical performance when stabilized by Li_2O units in the (2 × 2) tunnels (Fig. 1b).[18,19] In the class of solid electrolytes, the fast Na^+-ion conductor, β''-alumina ($Na_2O{\cdot}5.3Al_2O_3$, $\sigma \approx 0.3$ S cm^{-1} at 300 °C) consists of γ-Al_2O_3 spinel units that stabilize the Na^+-ion conducting (Na_2O) layers (Fig. 1c)[20,21] whereas $Ag_{44}I_{53}(C_{11}H_{30}N_3)_3$ ($44AgI{\cdot}3C_{11}H_{30}N_3I_3$) is an example of a Ag^+-ion conductor ($\sigma \approx 10^{-2}$ S cm^{-1} at 25 °C) in which triamine cationic units, $C_{11}H_{30}N_3^{3+}$, serve to quench and stabilize a highly conducting AgI component at room temperature (Fig. 1d).[22,23]

Layered $LiMO_2$ and spinel LiM_2O_4 compounds, in which M is typically an electrochemically active first row transition metal ion, such as manganese, nickel and cobalt, and stabilizing substituent cations, such as lithium, magnesium and aluminium, have close-packed structures with a close-packed interlayer distance of approximately 4.7 Å. Layered $Li_{1-x}MO_2$ structures tend to become unstable at high levels of delithiation, typically when x exceeds 0.5. When M = Co or Ni, the instability is attributed largely to the highly oxidizing nature of tetravalent cobalt and nickel, which results in the loss of oxygen and the migration of the transition metal ions to the lithium-depleted layer. When M = Mn, the delithiated structure transforms to a more stable spinel-type configuration, but this process degrades its high-potential (4 V) electrochemical performance.[24] In principle, however, a layered $Li_{1-x}MnO_2$ structure if kept intact over the full range of x ($0 < x < 1$) would yield an attractive 286 mAh g^{-1} between 4 V and 3 V.[25] (Note that the corresponding $Li_{1-x}MnO_2$ spinel system (*i.e.*, $Li_yMn_2O_4$; $0 < y < 2$, $y = 2 - 2x$) offers the same capacity, one half of which is delivered at ~4 V and the other half below 3 V.) Building on the concept of using a structural unit to stabilize electrochemically active materials, as described above, and guided by our earlier work in stabilizing MnO_2 compounds with Li_2O,[18,26] we adopted a similar strategy to stabilize layered $LiMO_2$ and LiM_2O_4 spinel electrodes by integrating a structurally compatible component that was electrochemically inactive (with respect to capacity generation) between 4 and 3 V. Our intention was to increase the stability of layered and spinel electrodes over a wider compositional range than was previously possible without compromising the power or cycle life of the cells.

Following our success in fabricating Li_2MnO_3-stabilized layered MnO_2 electrode structures by 1) leaching Li_2O from Li_2MnO_3 by acid treatment, 2) subsequent relithiation, either electrochemically in a lithium cell[27,28] or chemically with n-butyllithium,[29] and 3) recognizing the structural compatibility between $Li_2M'O_3$ (*e.g.*, Mn, Ti, Zr) and layered $LiMO_2$

and spinel LiM_2O_4 compounds,[30] we initiated efforts to synthesize structurally integrated 'layered–layered' $xLi_2M'O_3\cdot(1-x)LiMO_2$[31–33] and 'layered–spinel' $xLi_2M'O_3\cdot(1-x)LiM_2O_4$[33–35] compounds in which the $Li_2M'O_3$ component would act to provide additional stability to a layered $LiMO_2$ or a LiM_2O_4 spinel electrode over a wide operating voltage window of a lithium-ion cell, for example, 4.5 to 2.0 V. At present, 'layered–layered' electrodes appear to show the greatest promise of the two systems, particularly $xLi_2MnO_3\cdot(1-x)LiMO_2$ (M = Mn, Ni, Co) electrodes; the discussions that follow therefore focus on the structural, electrochemical and thermal properties of $xLi_2MnO_3\cdot(1-x)LiMO_2$ electrodes which emphasize their advantages over conventional lithium-ion battery electrodes.

3. Structurally integrated $xLi_2MnO_3\cdot(1-x)LiMO_2$ electrodes

3.1 Structural considerations

Schematic illustrations of idealized Li_2MnO_3 and $LiMO_2$ (M = Co, Ni, Mn) layered structures are shown in Fig. 2a and b, respectively. In $LiMO_2$ compounds, the average oxidation state of the M cations is three, as exemplified by Li_2MnO_3 ($Li[Li_{1/3}Mn_{2/3}]O_2$) in which tetravalent manganese and monovalent lithium comprise the M layer. Despite the variation in crystallographic space group symmetry brought about by differences in atomic and electronic configurations (monoclinic, $C2/m$ for Li_2MnO_3[36] and $LiMnO_2$;[37] trigonal, $R\bar{3}m$ for $LiCoO_2$[38] and $LiNiO_2$),[39] the close-packed layers in each of these compounds ($(001)_{monoclinic}$ and $(003)_{trigonal}$) have an interlayer spacing close to 4.7 Å. The compatibility of the close-packed layers allows the integration of a Li_2MnO_3 component with a $LiMO_2$ component at the atomic level, if one allows for some disorder between the Mn and M cations,[40] in much the same way that the hexagonally close-packed structures of β-MnO_2 (rutile-type) and ramsdellite-MnO_2 are integrated to form the composite structure of γ-MnO_2 (Fig. 1a). However, unlike γ-MnO_2[41] and layered–spinel[33] composite structures in which the respective rutile/ramsdellite and layered/spinel components can be readily distinguished from one another by high-resolution transmission electron microscopy (HRTEM), it is more difficult to differentiate two structurally compatible layered components with this technique, as illustrated in the HRTEM image of a $0.3Li_2MnO_3\cdot0.7LiMn_{0.5}Ni_{0.5}O_2$ composite structure in which the (001) and (003) lattice fringes of the Li_2MnO_3 and $LiMn_{0.5}Ni_{0.5}O_2$ components, respectively, are coincident (Fig. 3).

Both Li_2MnO_3 and $LiMO_2$ components of $xLi_2MnO_3\cdot(1-x)LiMO_2$ electrodes have rocksalt structures in which all

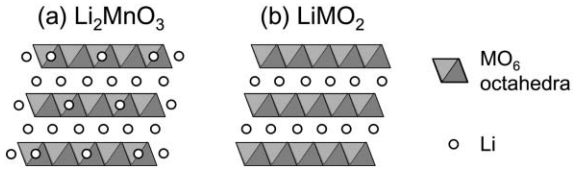

Fig. 2 Layered structures of a) Li_2MnO_3, b) $LiMO_2$ (M = Co, Ni, Mn).

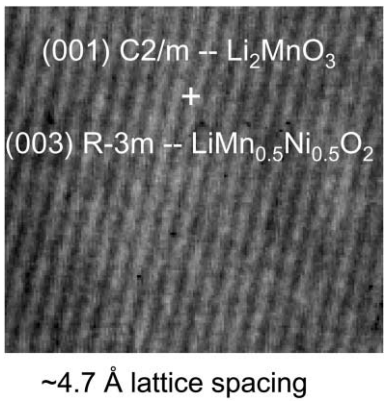

Fig. 3 TEM image of a $0.3Li_2MnO_3\cdot0.7LiMn_{0.5}Ni_{0.5}O_2$ electrode.

the octahedral sites of the (cubic) close-packed oxygen array are occupied. Between ~4.4 and 2.0 V *vs.* Li^0, the $LiMO_2$ component is electrochemically active and operates as a true insertion electrode. During charge, lithium extraction occurs with the concomitant oxidation of the M ions; the reverse process occurs during discharge. By contrast, the Li_2MnO_3 component is electrochemically inactive over this potential window, in the sense that it does not contribute to electrochemical capacity, because all the manganese ions are tetravalent and cannot be oxidized further. Lithium insertion into Li_2MnO_3, with a concomitant reduction of the manganese ions, is also prohibited because there are no energetically favorable interstitial sites for the guest ions. Under such conditions, the Li_2MnO_3 component acts as a stabilizing unit in the electrode structure. If, however, the electronically insulating Li_2MnO_3 regions are extremely small (nano-dimensional) and if they are distributed randomly throughout the composite structure, then these regions will function as solid electrolyte constituents in facilitating Li^+-ion transport between the capacity-generating $LiMO_2$ regions of the structure; in this respect, the Li^+-ion conductivity in a single-phase Li_2MnO_3 specimen has been reported to be in the range 10^{-6} to 10^{-3} S cm^{-1} between 18 and 400 °C with an activation energy of 44.87 kJ mol^{-1}.[42]

3.2 Nomenclature and the advantages of using a two-component $xLi_2MnO_3\cdot(1-x)LiMO_2$ notation

Because Li_2MnO_3 can be reformulated as $Li[Li_{1/3}Mn_{2/3}]O_2$, it is possible to normalize $xLi_2MnO_3\cdot(1-x)LiMO_2$ electrodes in standard layered notation as $Li_{1+(x/2+x)}M'_{1+(x/(2+x))}O_2$ in which M′ = Mn + M or, more simply, $Li_{1+y}M'_{1-y}O_2$ where $y = (x/(2+x))$. Layered $xLi_2MnO_3\cdot(1-x)LiMO_2$ electrodes can, therefore, be considered to be lithium-rich compounds with Mn^{4+} ions in the transition metal layers. Both notations have been used extensively in the literature and we use them interchangeably in this paper. For example, the lithium-rich $Li[Li_{0.2}Mn_{0.4}Cr_{0.4}]O_2$ electrode[43] can be represented in two-component notation as $0.4Li_2MnO_3\cdot0.4LiCrO_2$ whereas the systems $Li[Li_{x/3}Co_{1-x}Mn_{2x/3}]O_2$ for $0 < x < 1$,[44] and $Li[Li_{1/3-2x/3}Ni_xMn_{2/3-x/3}]O_2$ for $0 < x < 0.5$[45] can be rewritten as $(2x)Li_2MnO_3\cdot3(1-x)LiCoO_2$ and $(1-2x)Li_2MnO_3\cdot(3x)LiMn_{0.5}Ni_{0.5}O_2$, respectively, for the same ranges of x.

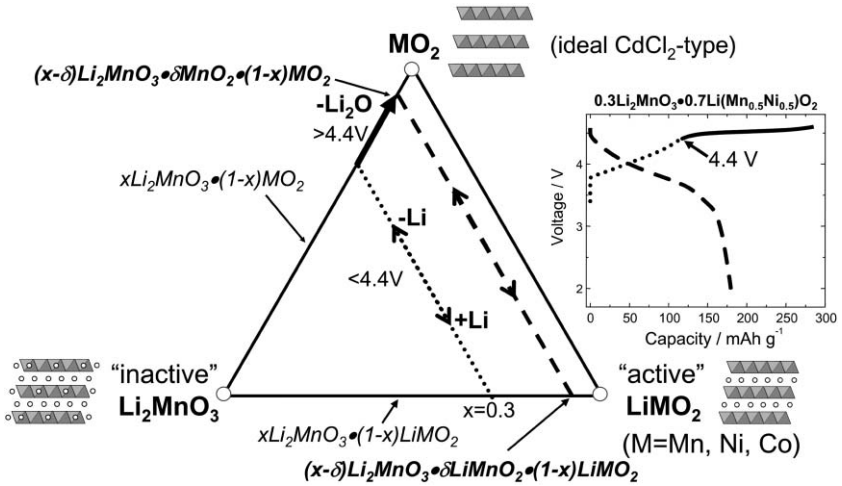

Fig. 4 Compositional phase diagram showing the electrochemical reaction pathways for a $xLi_2MnO_3\cdot(1-x)LiMO_2$ electrode.

There are several distinct advantages of using a two-component notation to describe $xLi_2MnO_3\cdot(1-x)LiMO_2$ electrodes because the Li_2MnO_3-like regions in these lithium-rich compounds play a major role in dictating their structural stability and electrochemical properties during charge and discharge. Furthermore, with this notation, it is possible to follow the electrochemical reactions of the $xLi_2MnO_3\cdot(1-x)LiMO_2$ electrodes on a Li_2MnO_3–$LiMO_2$–MO_2 compositional phase diagram as illustrated in Fig. 4, in which $0.3Li_2MnO_3\cdot 0.7LiMn_{0.5}Ni_{0.5}O_2$ (*i.e.*, M = $Mn_{0.5}Ni_{0.5}$) is used as the composition of a parent reference electrode. The corresponding profile of the initial charge/discharge cycle of a $Li/0.3Li_2MnO_3\cdot 0.7LiMn_{0.5}Ni_{0.5}O_2$ cell is also provided in Fig. 4. During the initial charge of the cell to approximately 4.4 V, lithium is extracted from the $LiMn_{0.5}Ni_{0.5}O_2$ component with a concomitant oxidation of the divalent nickel ions to the tetravalent state while the manganese 'spectator' ions remain tetravalent until the Li_2MnO_3–MO_2 ($Mn_{0.5}Ni_{0.5}O_2$) tie-line is reached. During this reaction, depletion of lithium ions from the lithium layer is compensated by the diffusion of lithium from octahedral sites in the manganese layer of the Li_2MnO_3 component to tetrahedral sites in the lithium-depleted layer thereby providing the additional binding energy necessary to maintain structural stability. This phenomenon has been observed experimentally by MAS NMR[46] and confirmed by theoretical calculations.[47] In this regard, therefore, the Li_2MnO_3 component acts as a reservoir of surplus lithium that can be used to stabilize the electrode structure at low lithium loadings. A schematic illustration of a lithium-depleted Li_2MnO_3-like unit is shown in Fig. 5. The co-existence of tetrahedral and octahedral lithium in the lithium-depleted layers gives the electrode structure two-dimensional, quasi-spinel-like features, reminiscent of the three-dimensional tetrahedral (8a)–octahedral (16c) interstitial network of the Mn_2O_4 spinel framework (space group $Fd\bar{3}m$),[48] suggesting that the lithium-depleted layers of $xLi_2MnO_3\cdot(1-x)Li_{1-y}MO_2$ electrodes provide an energetically favorable interstitial space for lithium, thereby ensuring fast reaction kinetics. Indeed, there have been reports that a 10–15% excess lithium in $Li_{1+x}M_{1-x}O_2$ electrodes enhances their rate capability,[49] consistent with our hypothesis. Furthermore, when fabricating layered $Li_{1+x}M_{1-x}O_2$ electrodes at elevated temperatures, particularly those containing nickel, the surplus lithium is beneficial for minimizing the contamination of the lithium layers by transition metal ions.[50]

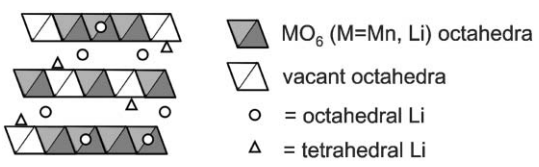

Fig. 5 Schematic illustration showing the 2-D spinel-like configuration in a delithiated Li_2MnO_3-like region of a $xLi_2MnO_3\cdot(1-x)LiMO_2$ electrode structure (M = Mn, Ni, Co).

If the electrochemical potential of a $Li/0.3Li_2MnO_3\cdot 0.7LiMO_2$ cell is raised above 4.4 V during charge, then further lithium can be extracted from the electrode as indicated by the solid line in the compositional phase diagram and electrochemical plot of the $Li/0.3Li_2MnO_3\cdot 0.7LiMO_2$ cell in Fig. 4. In this case, lithium is extracted from the Li_2MnO_3 component with the simultaneous release of oxygen;[32,45,51,52] the net loss from the $xLi_2MnO_3\cdot(1-x)MO_2$ is Li_2O. This reaction drives the composition of the electrode irreversibly towards the MO_2 apex of the Li_2MnO_3–$LiMO_2$–MO_2 phase diagram. Complete extraction of Li_2O from the Li_2MnO_3 component ($Li_2O\cdot MnO_2$) yields electrochemically active MnO_2. Reinsertion of lithium into the MnO_2 component is now possible with the concomitant reduction of manganese until the rocksalt stoichiometry $LiMnO_2$ is reached. Such an electrochemical activation process, therefore, provides an excellent method not only for tailoring the Li_2MnO_3 content and the amount of lithium in the Li_2MnO_3 reservoir required to stabilize delithiated $xLi_2MnO_3\cdot(1-x)LiMO_2$ electrodes, it also controls the amount of electrochemically active manganese in the electrodes after activation above 4.6 V.[52] The extraction of two Li^+ ions per Li_2MnO_3 unit on the initial charge and the reintroduction of only one Li^+ ion on the subsequent discharge into the resulting MnO_2 unit necessarily means that there must be an irreversible capacity loss on the

initial cycle, as clearly demonstrated in the electrochemical plot of Fig. 4. This phenomenon can, however, be advantageous, because it allows the possibility of using the surplus lithium in the parent $xLi_2MnO_3\cdot(1-x)LiMO_2$ electrode to offset any first-cycle, irreversible capacity loss that may be encountered at the negative electrode, notably the irreversible capacity losses that are typical of intermetallic anodes.[33]

3.3 The structural complexity of $xLi_2MnO_3\cdot(1-x)LiMO_2$ electrodes

The powder X-ray diffraction patterns of two $xLi_2MnO_3\cdot(1-x)LiMO_2$ systems in which M = $Mn_{0.5}Ni_{0.5}$ (x = 0, 0.3, 0.4, 0.5) and M = $Mn_{0.333}Ni_{0.333}Co_{0.333}$ (x = 0, 0.3. 0.5 and 0.7) are shown in Fig. 6a and b, respectively. Because of the remarkable structural compatibility of layered Li_2MnO_3, $LiMn_{0.5}Ni_{0.5}O_2$ and $LiMn_{0.333}Ni_{0.333}Co_{0.333}O_2$ compounds, all the strong diffraction peaks can be indexed to a pseudo-trigonal unit cell with $R\bar{3}m$ symmetry.[40] Several weak peaks between 21 and 25° 2θ (circled in Fig. 6a and b), which cannot be indexed to $R\bar{3}m$ symmetry, are consistent with the $LiMn_6$ cation ordering that occurs in the transition metal layers of Li_2MnO_3; they can be indexed to the monoclinic unit cell, $C2/m$, that characterizes Li_2MnO_3.[36] The magnitude of these weak peaks increases with the value of x, for both $xLi_2MnO_3\cdot(1-x)LiMn_{0.5}Ni_{0.5}O_2$ and $xLi_2MnO_3\cdot(1-x)LiMn_{0.333}Ni_{0.333}Co_{0.333}O_2$ systems, consistent with the increasing Li_2MnO_3-like character within the structures.

For low values of x in $xLi_2MnO_3\cdot(1-x)LiMO_2$ compounds, *i.e.*, when small amounts of excess lithium are used, the Li_2MnO_3-like features are sometimes difficult to discern in the X-ray diffraction patterns, particularly when cobalt is present, as in the $xLi_2MnO_3\cdot(1-x)LiMn_{0.333}Ni_{0.333}Co_{0.333}O_2$ system. In these instances, other analytical techniques, such as convergent beam electron diffraction (CBED)[53] and MAS NMR spectroscopy that probes local atomic environments[54,55] have to be used. Differences in the X-ray diffraction patterns of $xLi_2MnO_3\cdot(1-x)LiMn_{0.5}Ni_{0.5}O_2$ and $xLi_2MnO_3\cdot(1-x)LiMn_{0.333}Ni_{0.333}Co_{0.333}O_2$ systems were recently highlighted in a comparative study of layered, lithium-rich Li–Mn–Ni–O and Li–Mn–Ni–Co–O electrodes, in which the alternative notations $Li_{1+x}(Mn_{0.5}Ni_{0.5})_{1-x}O_2$ and $Li_{1+x}(Mn_{0.333}Ni_{0.333}Co_{0.333})_{1-x}O_2$ were used to define the amount of excess lithium in the electrode structures, for example, $Li_{1.024}[Mn_{0.333}Ni_{0.333}Co_{0.333}]_{0.976}O_2$ ($0.05Li_2MnO_3\cdot0.95LiMn_{0.298}Ni_{0.351}Co_{0.351}O_2$) and $Li_{1.048}[Mn_{0.333}Ni_{0.333}Co_{0.333}]_{0.952}O_2$ ($0.10Li_2MnO_3\cdot0.90LiMn_{0.256}Ni_{0.372}Co_{0.372}O_2$);[40] even at these low levels of excess lithium, evidence of Li_2MnO_3-like regions could be detected unequivocally by MAS NMR.

The complexity of structurally integrated $xLi_2MnO_3\cdot(1-x)LiMO_2$ compounds (M = Mn, Ni, Co) manifests itself in pronounced differences in the peak intensities of the weak ordering reflections in the XRD patterns of $Li_{1+x}(Mn_{0.5}Ni_{0.5})_{1-x}O_2$ and $Li_{1+x}(Mn_{0.333}Ni_{0.333}Co_{0.333})_{1-x}O_2$ compounds, as shown in Fig. 7a and b, respectively.[40] In $Li_{1+x}(Mn_{0.5}Ni_{0.5})_{1-x}O_2$ the ordering peaks increase with x, consistent with an increasing Li_2MnO_3 content, whereas for the $Li_{1+x}(Mn_{0.333}Ni_{0.333}Co_{0.333})_{1-x}O_2$ system the ordering peaks are significantly weaker and remain essentially unaltered as x increases. The structural complexity and differences in cation distributions between these compounds can be better understood by considering the schematic illustrations of idealized cation ordering arrangements in Li_2MnO_3 (Fig. 8a), $LiMn_{0.5}Ni_{0.5}O_2$ (Fig. 8b), $LiMn_{0.333}Ni_{0.333}Co_{0.333}O_2$ (Fig. 8d), and proposed models for cation arrangements in the highly complex composite structures of lithium-rich $Li_{1+x}(Mn_{0.5}Ni_{0.5})_{1-x}O_2$ (Fig. 8c) and $Li_{1+x}(Mn_{0.333}Ni_{0.333}Co_{0.333})_{1-x}O_2$ (Fig. 8e) compounds. Representative X-ray diffraction patterns of each of the compounds are provided in Fig. 8(a)–(e), to aid in the discussion that follows.

a) Li_2MnO_3. Fig. 8a shows a slice of the manganese-rich layer of the Li_2MnO_3 rock salt structure ($C2/m$ symmetry)

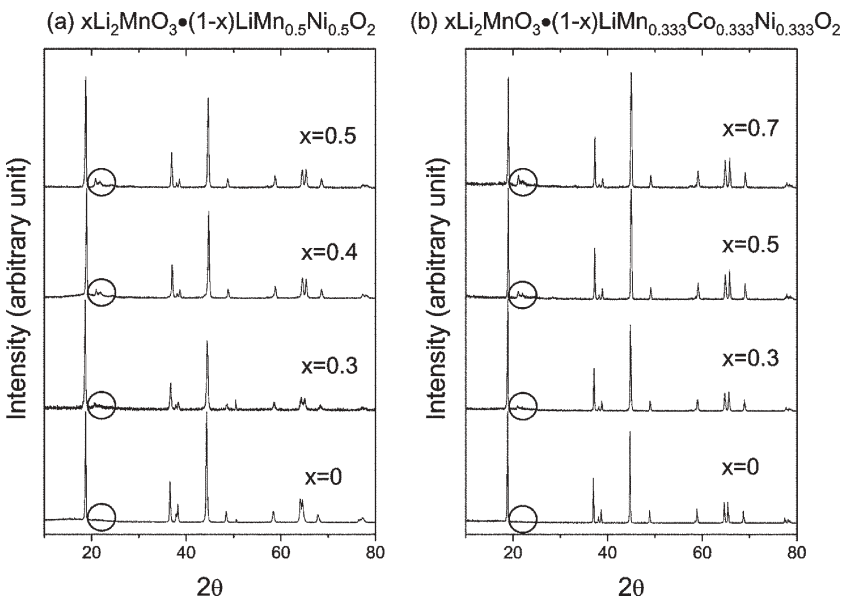

Fig. 6 X-Ray diffraction patterns of (a) $xLi_2MnO_3\cdot(1-x)LiMn_{0.5}Ni_{0.5}O_2$ for x = 0, 0.3, 0.4, 0.5; and (b) $xLi_2MnO_3\cdot(1-x)LiMn_{0.333}Ni_{0.333}Co_{0.333}O_2$ for x = 0, 0.3, 0.5, 0.7.

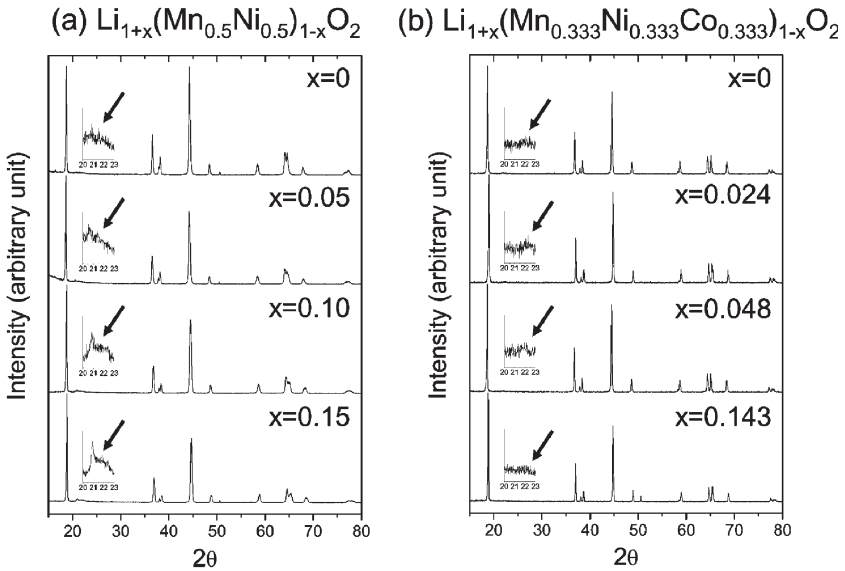

Fig. 7 X-Ray diffraction patterns of (a) $Li_{1+x}(Mn_{0.5}Ni_{0.5})_{1-x}O_2$ for $x = 0$, 0.05, 0.10 and 0.15; and (b) $Li_{1+x}(Mn_{0.333}Ni_{0.333}Co_{0.333})_{1-x}O_2$ for $x = 0$, 0.024, 0.048 and 0.143 [after ref. 40]. Figures reproduced from ref. 40 with permission from Elsevier.

which contains 67% Mn and 33% Li; the manganese and lithium ions occupy all the octahedral sites of the layer; the oxygen ions at the apices of the octahedra are represented by small dots. The lithium layers are located immediately above and below the manganese-rich plane. In this idealized Li_2MnO_3 structure, six MnO_6 octahedra surround every LiO_6 octahedron, giving rise to a hexagonal $LiMn_6$ nearest-neighbor unit in the manganese-rich plane that, together with the nearest-neighbor lithium ions in adjacent layers, represents the building block of Li_2MnO_3; it is this cation ordering arrangement that gives rise to the relatively weak peaks at approximately 21–25° 2θ in the X-ray diffraction pattern of Li_2MnO_3 (Fig. 8a).

b) $LiMn_{0.5}Ni_{0.5}O_2$. Computational studies by Van der Ven *et al.* have revealed that the low energy cation arrangement in $LiMn_{0.5}Ni_{0.5}O_2$ has a flower pattern, as depicted in Fig. 8b.[56] In this configuration, approximately 8% of the lithium ions are located in the transition metal layer with a corresponding amount of nickel in the lithium layer; contamination of the lithium layers by nickel has been corroborated by experiment.[57] The cation distribution in the ideal flower structure of $LiMn_{0.5}Ni_{0.5}O_2$ can, therefore, be represented $Li_{0.92}Ni_{0.08}$-$[Mn_{0.50}Ni_{0.42}Li_{0.08}]O_2$. It has also been established by X-ray absorption near edge spectroscopy (XANES) that, in $LiMn_{0.5}Ni_{0.5}O_2$, the manganese ions are tetravalent and nickel ions, divalent.[58] Furthermore, MAS NMR studies of $LiMn_{0.5}Ni_{0.5}O_2$ and $Li[Li_{1/3-2x/3}Ni_xMn_{2/3-x/3}]O_2$ (alternatively, $(1-2x)Li_2MnO_3{\cdot}(3x)LiMn_{0.5}Ni_{0.5}O_2$) structures have shown that the lithium ions cluster preferentially around the tetravalent manganese ions to form $LiMn_6$ units in order to satisfy Pauling's local electrical neutrality rule thereby imparting Li_2MnO_3-like character to the structures.[59] These NMR studies also demonstrated that some exchange occurs between Ni and the Mn of the $LiMn_6$ units to yield, for example, $LiMn_5Ni$ units. In practice, a perfectly ordered flower configuration is unlikely to be generated during high temperature synthesis. Indeed, it has been reported that the $LiMn_{0.5}Ni_{0.5}O_2$ structure is characterized by crystallographic imperfections, such as disorder in the stacking sequence.[60] Furthermore, the X-ray diffraction patterns of most $LiMn_{0.5}$-$Ni_{0.5}O_2$ samples contain weak peaks at 21–25° 2θ, providing evidence of short range order of the LiM_6 units of a Li_2MnO_3-like component in the transition metal layers (see XRD pattern inset in Fig. 8b) consistent with the work of others.[60,61]

c) $xLi_2MnO_3{\cdot}(1-x)LiMn_{0.5}Ni_{0.5}O_2$ and $Li_{1+x}(Mn_{0.5}$-$Ni_{0.5})_{1-x}O_2$ compounds ($x > 0$). When Li_2MnO_3 units are integrated into $LiMn_{0.5}Ni_{0.5}O_2$ ($xLi_2MnO_3{\cdot}(1-x)LiMn_{0.5}$-$Ni_{0.5}O_2$), or if excess lithium is added to a $LiMn_{0.5}Ni_{0.5}O_2$ composition at the expense of the $Mn_{0.5}Ni_{0.5}$ component to maintain a rocksalt stoichiometry $Li_{1+x}(Mn_{0.5}Ni_{0.5})_{1-x}O_2$ ($0 < x \leqslant 0.2$), which at $x_{max} = 0.2$ has the alternative notation $0.4Li_2MnO_3{\cdot}0.4LiNiO_2$, then it stands to reason that both $xLi_2MnO_3{\cdot}(1-x)LiMn_{0.5}Ni_{0.5}O_2$ and $Li_{1+x}(Mn_{0.5}Ni_{0.5})_{1-x}O_2$ systems should show increasing Li_2MnO_3-like character with increasing x. This premise is confirmed by the X-ray diffraction patterns in Fig. 6a and 7a, respectively. Note that in the $Li_{1+x}(Mn_{0.5}Ni_{0.5})_{1-x}O_2$ system, increasing the lithium content at the expense of the $Mn_{0.5}Ni_{0.5}$ content must of necessity increase the average nickel-ion oxidation state from 2+ ($x = 0$) to 3+ ($x = 0.2$). If the lithium ions remain clustered to the tetravalent manganese ions in $Li_{1+x}(Mn_{0.5}Ni_{0.5})_{1-x}O_2$ compounds as x increases, then a picture of an integrated Li_2MnO_3–$LiNiO_2$ composite structure clearly emerges, as depicted in Fig. 8c for $x \approx 0.1$, in which twelve lithium ions have been added to the flower pattern at the expense of six manganese ions and six nickel ions.

A similar approach to that adopted above can be used to visualize possible atomic configurations in $xLi_2MnO_3{\cdot}$ $(1-x)LiMn_{0.333}Ni_{0.333}Co_{0.333}O_2$ or $Li_{1+x}(Mn_{0.333}Ni_{0.333}$-$Co_{0.333})_{1-x}O_2$ electrode structures.

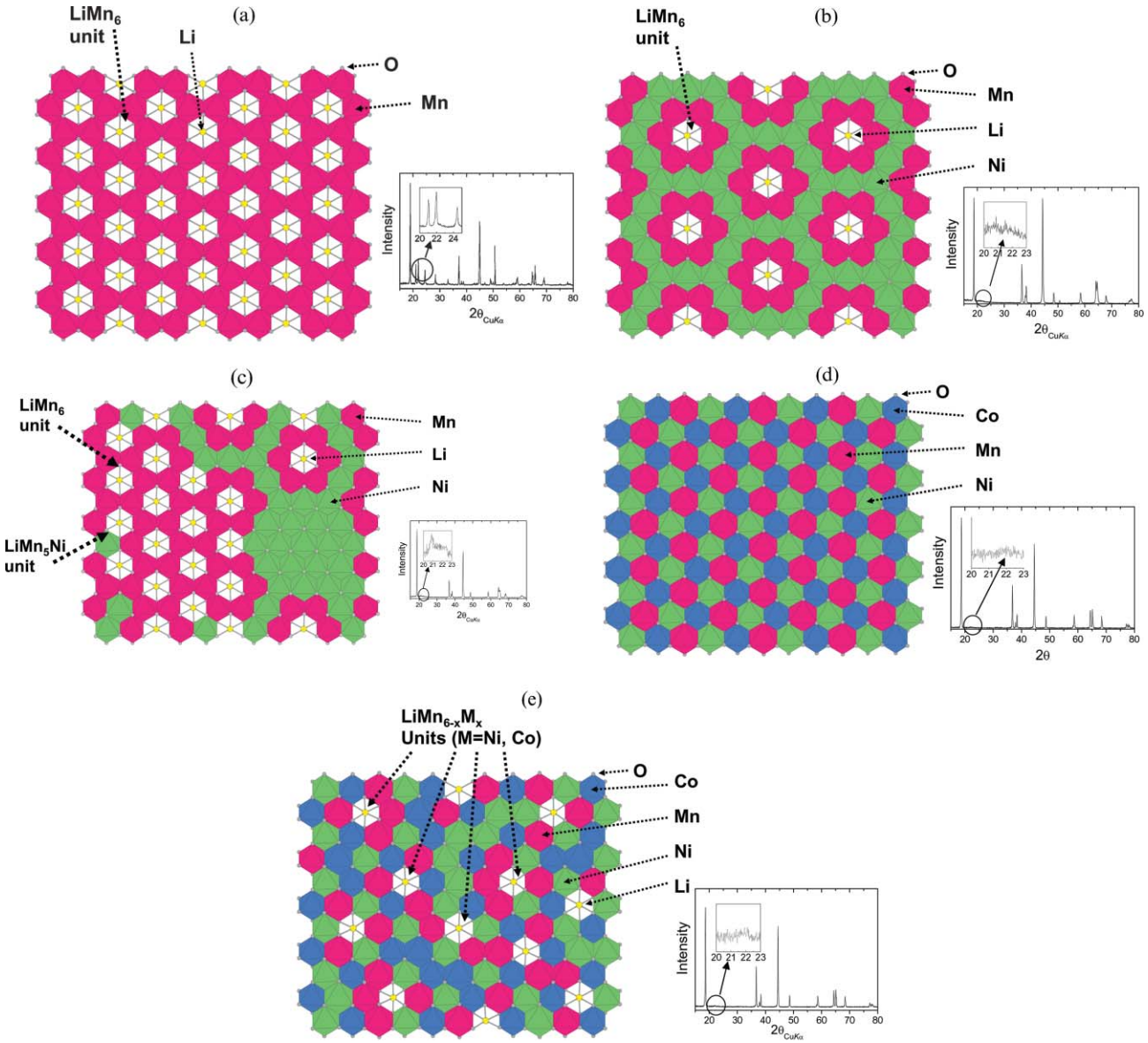

Fig. 8 Schematic structural illustrations and XRD patterns highlighting peaks corresponding to $LiMn_{6-x}M_x$ (M = Ni, Co) cation configurations in (a) Li_2MnO_3; (b) $LiMn_{0.5}Ni_{0.5}O_2$; (c) $Li_{1+x}(Mn_{0.5}Ni_{0.5})_{1-x}O_2$; (d) $LiMn_{0.333}Ni_{0.333}Co_{0.333}O_2$; and (e) $Li_{1+x}(Mn_{0.333}Ni_{0.333}Co_{0.333})_{1-x}O_2$.

d) $LiMn_{0.333}Ni_{0.333}Co_{0.333}O_2$. An idealized representation of the $LiMn_{0.333}Ni_{0.333}Co_{0.333}O_2$ structure is shown in Fig. 8d. The 1 : 1 : 1 ratio of manganese, nickel and cobalt in the transition metal layers allows for an ordered arrangement of atoms and the maintenance of trigonal symmetry, characteristic of the prototypic layered $LiCoO_2$ electrode.[4] The virtual absence of peaks in the 21–25° 2θ range of the X-ray diffraction pattern of $LiMn_{0.333}Ni_{0.333}Co_{0.333}O_2$ (Fig. 8d) confirms that there is negligible lithium in the transition metal layers. Although it has been reported from XANES analyses that the manganese and nickel ions in $LiMn_{0.333}Ni_{0.333}Co_{0.333}O_2$ appear to adopt tetravalent and divalent oxidation states, respectively,[62] the regular arrangement of Ni–Co, Mn–Co and Mn–Ni nearest neighbors in this structure makes it highly likely that the trivalent cobalt ions will disturb the electronic interactions and charge ordering between the manganese and nickel ions.

e) $xLi_2MnO_3\cdot(1-x)LiMn_{0.333}Ni_{0.333}Co_{0.333}O_2$ and $Li_{1+x}(Mn_{0.33}Ni_{0.33}Co_{0.33})_{1-x}O_2$ compounds. Integration of Li_2MnO_3 with $LiMn_{0.333}Ni_{0.333}Co_{0.333}O_2$ to form $xLi_2MnO_3\cdot(1-x)LiMn_{0.333}Ni_{0.333}Co_{0.333}O_2$ compounds increases the magnitude of the characteristic Li_2MnO_3 peaks at low 2θ values with increasing x, as expected (Fig. 6b). In the $Li_{1+x}(Mn_{0.333}Ni_{0.333}Co_{0.333})_{1-x}O_2$ system, the addition of lithium at the expense of the $(Mn_{0.333}Ni_{0.333}Co_{0.333})$ component, in principle, should also increase the Li_2MnO_3 content in the structure, yielding a composition $Li_2MnO_3\cdot 2LiNi_{0.5}Co_{0.5}O_2$ at $x_{max} = 1/7$ (0.143) in which the manganese ions are tetravalent and the nickel and cobalt ions, trivalent. However, in this instance, the magnitude of the X-ray diffraction peaks at low 2θ remains weak and it is virtually unaffected by increasing the lithium content, x (Fig. 7b), the reason for which can be understood by reference to a proposed schematic representation of the cation disorder in a

$Li_{1+x}(Mn_{0.333}Ni_{0.333}Co_{0.333})_{1-x}O_2$ structure in which $x \approx 0.1$ (Fig. 8e). In this illustration, following the same procedure used for the $Li_{1+x}(Mn_{0.5}Ni_{0.5})_{1-x}O_2$ electrode structure in Fig. 8c, twelve lithium ions have been added to the pattern of the $LiMn_{0.333}Ni_{0.333}Co_{0.333}O_2$ structure (Fig. 8d) at the expense of four manganese, four nickel and four cobalt ions. It is immediately evident that in this $Li_{1+x}(Mn_{0.333}Ni_{0.333}Co_{0.333})_{1-x}O_2$ structure, which has significantly less manganese than in the corresponding $Li_{1+x}(Mn_{0.5}Ni_{0.5})_{1-x}O_2$ structure (Fig. 8c), it is more difficult to cluster the lithium distinctly around the manganese ions to generate short-range order in the $LiMn_{6-x}M_x$ hexagonal units (M = Ni, Co). Fig. 8c and e clearly illustrate that $xLi_2MnO_3{\cdot}(1-x)LiMO_2$ (M = Mn, Ni, Co) structures, particularly those containing cobalt, are extremely complex, and that introduction of Co^{3+} ions leads to increased disorder and isolation of the $LiMn_{6-x}M_x$ (M = Ni, Co) regions, rendering them almost amorphous to X-ray diffraction (Fig. 8e), in contrast to their greater visibility and short-range order in lithium-rich Li–Mn–Ni–O electrode structures (Fig. 8c).[40]

4. Thermal stability

The introduction of manganese into layered $LiMO_2$ electrode structures containing cobalt and nickel has a profound and positive effect on the thermal stability of the delithiated electrodes, as demonstrated in recent comparative studies of a lithium–nickel–cobalt–aluminium–oxide electrode, $LiNi_{0.80}Co_{0.15}Al_{0.05}O_2$ ('NCA') and a lithium-rich lithium–nickel–cobalt–manganese–oxide electrode, $Li_{1.10}(Mn_{0.333}Ni_{0.333}Co_{0.333})_{0.90}O_2$ ('NCM') (alternatively, $0.22Li_2MnO_3{\cdot}0.78LiMn_{0.143}Ni_{0.429}Co_{0.429}O_2$).[63] Differential scanning calorimetry (DSC) data have shown not only that the heat generated on heating a charged $Li_{1-x}Ni_{0.8}Co_{0.15}Al_{0.05}O_2$ electrode in a 1.2 M $LiPF_6$ ethylene carbonate (EC)–propylene carbonate (PC)–dimethyl carbonate (DMC) (1 : 1 : 1) electrolyte (1065 J g^{-1}) is significantly greater than that generated by a similarly charged $Li_{1.10}(Mn_{0.333}Ni_{0.333}Co_{0.333})_{0.90}O_2$ electrode, but also that the onset reaction temperature for heat release is significantly higher for the latter electrode (~275 °C) compared to $Li_{1-x}Ni_{0.80}Co_{0.15}Al_{0.05}O_2$ (~200 °C).[63] More recent, unpublished data have demonstrated that $xLi_2MnO_3{\cdot}(1-x)LiMO_2$ (M = Mn, Ni, Co) electrodes generate even less heat when the electrodes contain a high manganese content ($x \sim 0.5$),[64] making these electrodes excellent candidates for enhancing the safety features of charged lithium–cobalt–nickel–oxide electrodes.

5. Electrochemistry and cycling stability

Layered $xLi_2MnO_3{\cdot}(1-x)LiMO_2$ (M = Mn, Ni, Co) electrodes can provide exceptionally high electrochemical capacities by activating the Li_2MnO_3 component above 4.4 V *vs.* Li^0; the capacity and cycling stability is dependent on the value of x and the relative amounts of manganese, nickel and cobalt in the $LiMO_2$ component. It has been demonstrated in several independent studies that these electrodes can deliver their theoretical capacities, which reach ~260 mAh g^{-1} (calculated from the mass of the parent $xLi_2MnO_3{\cdot}(1-x)LiMO_2$ electrode before electrochemical activation) when charged and discharged between 5 and 2 V *vs.* Li^0.[65–67] If a low current rate (0.05 mA cm^{-2}), an elevated operating temperature (~50 °C) and a relatively high value of x (0.5–0.7) are used, then an anomalously high capacity in excess of the theoretical value, typically 280–300 mAh g^{-1}, can be obtained; in most cases, the capacity declines during the early cycles of the cell to the theoretical value and lower.[65] For example, the voltage profiles for the first two charge/discharge cycles of a $Li/0.3Li_2MnO_3{\cdot}0.7LiMn_{0.5}Ni_{0.5}O_2$ cell at room temperature are shown in Fig. 9a. A peak at 4.53 V in the dQ/dV plot of the initial charge reaction, which is absent during the subsequent charge, is consistent with the irreversible removal of Li_2O from, electrochemical activation of, the Li_2MnO_3 component that occurs on the voltage plateau at 4.5–4.6 V. On the initial charge to 5 V, the electrode delivers 353 mAh g^{-1}, in excellent agreement with the theoretical value of 341 mAh g^{-1} for the removal of all the lithium (1.3 Li^+) if some electrolyte oxidation is taken into account. However, on the subsequent discharge to 2.0 V, 287 mAh g^{-1} is recovered from the electrode; this value is in excess of the theoretical capacity from a fully delithiated $0.3MnO_2{\cdot}0.7Mn_{0.5}Ni_{0.5}O_2$ electrode, namely 263 mAh g^{-1}, when the mass of the parent electrode is used for the calculation. The discharge capacity decreases steadily on cycling the cell, reaching the theoretical value after a few cycles. Although the precise reasons for the anomalous behavior of $xLi_2MnO_3{\cdot}(1-x)LiMO_2$ electrodes have not yet been determined, the excess capacity has been attributed tentatively to capacitive effects, electrolyte-related

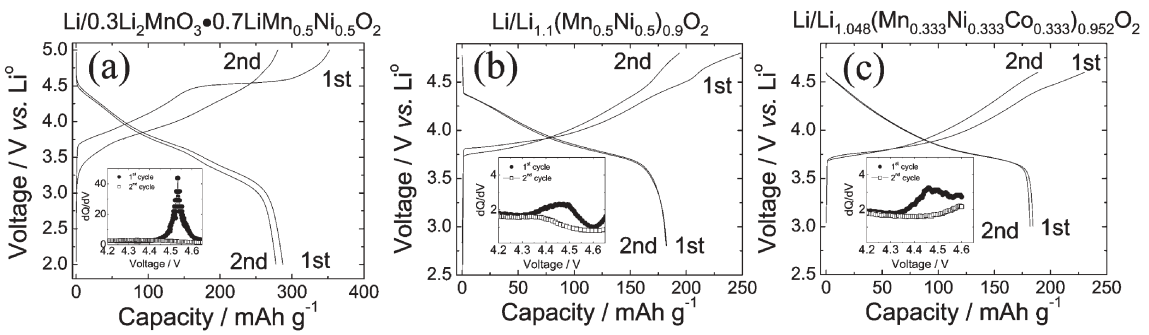

Fig. 9 Initial two charge/discharge voltage profiles and corresponding dQ/dV plots (inset) of (a) a $Li/0.3Li_2MnO_3{\cdot}0.7LiMn_{0.5}Ni_{0.5}O_2$ cell; (b) a $Li/Li_{1.1}(Mn_{0.5}Ni_{0.5})_{0.9}O_2$ cell; and (c) a $Li/Li_{1.048}(Mn_{0.333}Ni_{0.333}Co_{0.333})_{0.952}O_2$ cell [after ref. 40]. Figures reproduced from ref. 40 with permission from Elsevier.

phenomena and possible electronic contributions from the oxygen ions.[65]

If lower levels of excess lithium are used, when the Li_2MnO_3-like (LiM_6) units are dispersed more widely over the $xLi_2MnO_3{\cdot}(1-x)LiMO_2$ electrode structures, then the magnitude of the electrochemical activation peak at approximately 4.5 V in the dQ/dV plots, characteristic of irreversible lithium extraction from the transition metal layers, is significantly reduced, as expected, as shown in Fig. 9b and c for a $Li/0.22Li_2MnO_3{\cdot}0.78LiMn_{0.357}Ni_{0.643}O_2$ ($Li_{1.10}(Mn_{0.5}Ni_{0.5})_{0.90}O_2$) cell and a $Li/0.1Li_2MnO_3{\cdot}0.9LiMn_{0.256}Ni_{0.372}Co_{0.372}O_2$ ($Li_{1.048}(Mn_{0.333}Ni_{0.333}Co_{0.333})_{0.952}O_2$) cell, respectively.

What is remarkable about the electrochemical activation of $xLi_2MnO_3{\cdot}(1-x)LiMO_2$ electrodes at >4.4 V is that the overall layered configuration of the structure remains intact despite the release of oxygen from the electrode surface during this process.[51] However, the extensive removal of Li_2O appears to damage the electrode surface during electrochemical activation because the cell impedance increases and the capacity declines steadily on cycling, particularly when higher current rates are used. This is apparent in the $Li/0.1Li_2MnO_3{\cdot}0.9LiMn_{0.256}Ni_{0.372}Co_{0.372}O_2$ ($Li_{1.048}(Mn_{0.333}Ni_{0.333}Co_{0.333})_{0.952}O_2$) cell, in which there is a steady decline in capacity on cycling the cell between 4.6–3.0 V when the current rate is increased five-fold after the two initial cycles (see next section, Fig. 11a).

6. Preconditioned and surface-stabilized $xLi_2MnO_3{\cdot}(1-x)LiMO_2$ electrodes

6.1 Acid treatment to combat first-cycle irreversible capacity loss

Although the first-cycle irreversible capacity loss that occurs during the electrochemical activation of a $xLi_2MnO_3{\cdot}(1-x)LiMO_2$ cathode can be used to offset the first cycle capacity loss at the anode, the extent of the cathode capacity loss may be more than that encountered at the anode, particularly if the parent $xLi_2MnO_3{\cdot}(1-x)LiMO_2$ electrode contains a high Li_2MnO_3 content (x). Alternatively, instead of electrochemical activation, a chemical preconditioning step can be used to activate the $xLi_2MnO_3{\cdot}(1-x)LiMO_2$ electrode by leaching Li_2O from the Li_2MnO_3 component with acid.[68,69] The success of this approach has been demonstrated in lithium half cells in which $xLi_2MnO_3{\cdot}(1-x)LiMO_2$ electrodes, after being preconditioned with 0.1 M HNO_3 (initial pH $\approx$ 1), operate with 100% coulombic efficiency on the initial charge/discharge cycle.[69] However, it was clear from these studies that, despite the effectiveness of the technique to eliminate the first-cycle irreversible capacity loss, the coulombic efficiency of acid-treated electrodes on subsequent cycles is inferior to untreated electrodes, as shown in Fig. 10a and b,[69] suggesting that the preconditioning reaction damages the electrode as a result of possible H^+–Li^+ ion-exchange or etching/dissolution reactions at the surface.

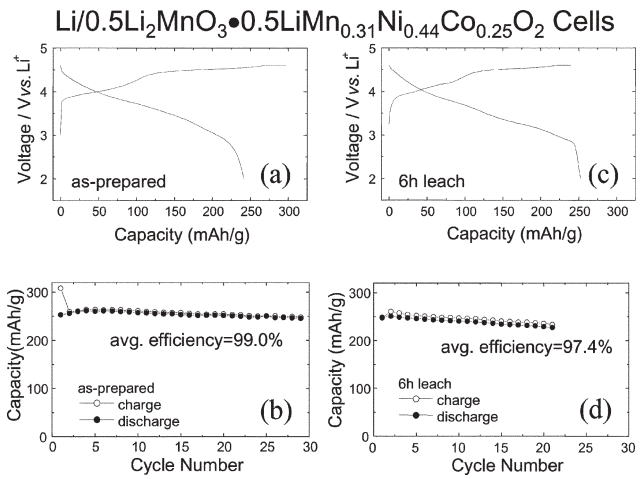

Fig. 10 Initial charge and discharge profiles and capacity *vs.* cycle number plots of lithium cells with an as-prepared $0.5Li_2MnO_3{\cdot}0.5LiMn_{0.31}Ni_{0.44}Co_{0.25}O_2$ electrode (a, b), and an acid-treated electrode (6 h leach) [after ref. 69]. Figures reproduced from ref. 69 with permission from The Electrochemical Society.

6.2 H^+–Li^+ ion exchange *vs.* dissolution reactions—computational studies

Because H^+–Li^+ ion exchange and dissolution reactions can damage the electrochemical properties of lithium insertion electrodes, lithium-ion battery electrolyte salts and solvents need to be pure and dry. For example, it is well known that a small amount of water, even a few ppm, in a $LiPF_6$-based electrolyte will hydrolyze the electrolyte salt to generate HF and POF_3[70] and that the acidic (HF) species can attack metal oxide electrodes, leading to surface dissolution. This phenomenon is particularly well known for $LiMn_2O_4$ spinel electrodes.[71,72] Reactions of lithium metal oxides with acid can also lead to H^+–Li^+ ion exchange reactions that can trigger structural changes, as observed in the $Li[Li_{1/3}Mn_{2/3}]O_2$ (Li_2MnO_3) to $H[Li_{1/3}Mn_{2/3}]O_2$ transition.[73,74]

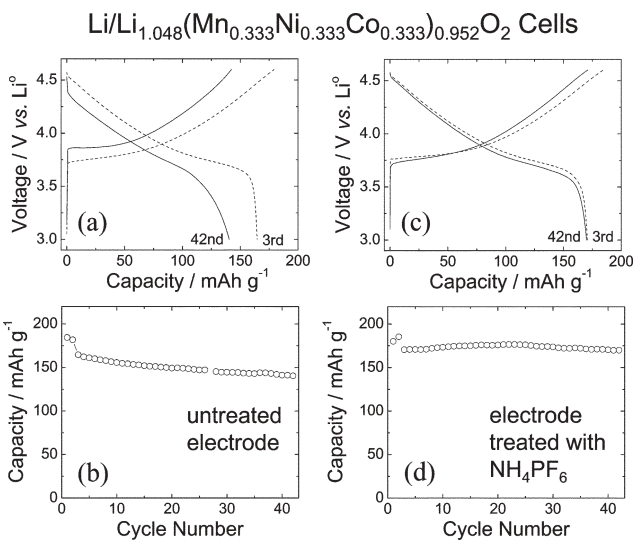

Fig. 11 Charge/discharge voltage profiles for the 3rd and 42nd cycles and capacity *vs.* cycle number plots of lithium half cells (metallic Li anode) with, (a) and (b), an untreated $Li_{1.048}(Mn_{0.33}Ni_{0.33}Co_{0.33})_{0.952}O_2$ electrode and, (c) and (d), an electrode preconditioned with a 2.4×10^{-3} M NH_4PF_6 solution (pH $\approx$ 6.5) prior to cell assembly, respectively.

First principles density functional theory calculations can be used to gain insight into the acid-promoted dissolution and proton–lithium ion-exchange reactions of lithium metal oxide electrodes.[75] In this respect, theoretical studies of $xLi_2MnO_3 \cdot (1-x)LiMO_2$ electrodes have been initiated at Argonne, in which acid reactions with individual Li_2MnO_3 and $LiMO_2$ components, such as $LiCoO_2$, were first considered. Despite the preliminary nature of this work, it is pertinent to make a brief comment on the results achieved thus far. Ideally, predictions of reaction rates would be most desirable because they would indicate which reactions are physically relevant at a given temperature and pH. Unfortunately, the atomic configurations of the activated (transition) states for liquid–solid reactions (unlike, *e.g.*, for some gas-phase and catalyzed gas-phase reactions)[76] are generally unknown, and may involve a vast number of atomic coordinates, which makes detailed calculations impractical at this time. Instead, we have focused on thermodynamic properties, particularly the free energy difference ΔG between products and reactants, which drives the reactions, and which is more accessible to computation.

For example, a scheme for the dissolution of layered $LiCoO_2$ in acid is:[77]

$$2\ LiCoO_2(s) + 4\ H^+(aq) \rightarrow CoO_2(s) + 2\ H_2O(aq) + Co^{2+}(aq) + 2\ Li^+(aq) \quad (1)$$

whereas the ion exchange reaction is

$$LiCoO_2 + H^+ \rightarrow HCoO_2 + Li^+ \quad (2)$$

In the case of Li_2MnO_3 ($Li[Li_{1/3}Mn_{2/3}]O_2$), it is known that ion exchange in the lithium layers occurs first

$$Li[Li_{1/3}Mn_{2/3}]O_2 + H^+ \rightarrow H[Li_{1/3}Mn_{2/3}]O_2 + Li^+ \quad (3)$$

followed by the dissolution/removal of Li^+ ions and H_2O[73]

$$1/3\ H^+ + H[Li_{1/3}Mn_{2/3}]O_2 \rightarrow 2/3\ MnO_2(s) + 2/3\ H_2O(aq) + 1/3Li^+(aq) \quad (4)$$

Although these schemes are somewhat idealized (for example, the extent of Li^+ dissolution in reaction (4) is taken to completion and the possible role of the anion in the dissolution is omitted), they have the benefit of tractability. The total energies of the solid phases can be evaluated with the VASP local density functional theory code, at the GGA+U level.[78–80] Empirical hydration free energies of the aqueous species are used in the calculations[81] and some corrections are required to reconcile the different free energy conventions used for solid phases and for aqueous solution species.[75] Calculations of the vibrational free energy contributions for the solid phases, which have not yet been included, are now in progress.[82]

Preliminary results indicate that reactions (1)–(3) above are all exothermic. Furthermore, our simulations for the H^+–Li^+ ion exchange process suggest that activation barriers are negligible in the shear transformation from the original monoclinic $C2/m$ symmetry of Li_2MnO_3 to the $R\bar{3}m$ symmetry of the protonated structure, and that the shear modulus of the transformed system $H[Li_{1/3}Mn_{2/3}]O_2$ is well below that of the original Li_2MnO_3. The reaction free energy driving the subsequent dissolution of $H[Li_{1/3}Mn_{2/3}]O_2$ is somewhat smaller (per proton) than for the original protonation.

For both $LiCoO_2$ and $LiMn_2O_4$, the magnitude of the driving force $|\Delta G|$ is much larger for dissolution than for ion exchange, but with delithiation and decreasing concentrations of transition metal ions in the 3+ oxidation state, the driving force for dissolution decreases, as expected for a disproportionation reaction. Likewise, by substitution of Li on the Mn sublattice, the composition $Li_4Mn_5O_{12}$ may be approached, and $|\Delta G|$ diminishes proportionally to the decrease in trivalent Mn, and ion exchange becomes more prominent.[83]

Calculations for a wide variety of oxide hosts have shown that H^+–Li^+ ion exchange is most favorable in layered compounds such as $LiCoO_2$ and Li_2MnO_3, and least favored in structures with complex oxygen polyhedra such as olivine $LiFePO_4$. This behavior is plausible, since the bonding in layered structures can readjust from Li to H by a shift in interlayer spacing, and/or interlayer shear, without significant distortion of the MO_6 octahedra.[84] The accommodation of H requires much more profound rearrangements and is energetically unfavorable for systems with complex octahedra, such as $LiFePO_4$.

For all the calculations described above, aqueous ionic species at infinite dilution were considered, whereas the dependence of $|\Delta G|$ on pH and T was not considered. For at least some transition metal oxides, $\Delta G(\mathrm{pH},T)$ may vanish along an equilibration line in (pH,T) space. In that case, the direction of the reaction could be reversed by tuning the pH (or temperature) of the system on either side of the equilibration line. The ability to predict the locus of this equilibration line would be a stringent test of the accuracy of the first principles free energy calculations, as well as the standard hydration free energies. Nevertheless, this theoretical approach may well play an important role in determining the conditions under which highly complex, integrated $xLi_2MnO_3 \cdot (1-x)LiMO_2$ electrode structures should be chemically preconditioned with acid to offset any damaging consequences of competing dissolution/ion-exchange reactions.

6.3 Fluorinated electrodes

Given the strong oxidizing character of chemically or electrochemically delithiated lithium metal oxide structures containing tetravalent cobalt, nickel and manganese, and their susceptibility to acid attack, whether by protonation or dissolution, it is not surprising that the surfaces of charged $Li_{1-x}MO_2$ electrode particles are reactive and unstable in a $LiPF_6$/organic solvent electrolyte environment. There have been many attempts over recent years to lower the surface reactivity of charged electrode particles by applying a coating, for example, a lithium borate glass,[85] Al_2O_3, TiO_2,[86] $AlPO_4$,[87] ZrO_2,[86,88,89] SiO_2,[89] or by using fluorinating agents, such as NH_4HF_2[90] and AlF_3[91] to provide robust surfaces and structures that can withstand the harsh chemical and electrochemical environments within a high-voltage lithium-ion cell. In particular, fluorinated electrodes with both spinel structures and layered structures[13–16] have shown significantly enhanced capacity and capacity retention on electrochemical cycling.

For example, the surface of $xLi_2MnO_3\cdot(1-x)LiMO_2$ electrode particles can be passivated effectively by washing the electrodes in mildly acidic fluoride solutions, such as 2.4×10^{-3} M NH_4PF_6 or $(NH_4)_3AlF_6$ (pH = 6.0–6.5),[92] prior to cell assembly. This approach allows the electrode particle surface to be etched and passivated with minimal damage relative to the damage caused by stronger acidic solutions, such as 0.1 M HNO_3 (initial pH $\approx$ 1).[69] The significant improvement in capacity and capacity retention obtained by fluorinating a $0.1Li_2MnO_3\cdot0.9LiMn_{0.256}Ni_{0.372}Co_{0.372}O_2$ ($Li_{1.048}(Mn_{0.333}Ni_{0.333}Co_{0.333})_{0.952}O_2$) electrode in a 2.4×10^{-3} M NH_4PF_6 solution is clearly demonstrated in Fig. 11(a)–(d) and 12(a)–(d) which compare the electrochemical behavior of untreated and fluorinated electrodes in lithium half cells and full cells, respectively, when operated continuously between 4.6 and 3.0 V. Of particular significance is that the fluorinated electrodes in the full cell tests (Fig. 12c and d) show excellent capacity retention and stability despite increasing the current rate five fold from 0.1 mA cm^{-2} to 0.5 mA cm^{-2} after the first two cycles. These data bode well for the future development of surface stabilized, high capacity and high rate $xLi_2MnO_3\cdot(1-x)LiMO_2$ electrodes.

7. Conclusions

Structurally integrated $xLi_2MnO_3\cdot(1-x)LiMO_2$ (M = Mn, Ni, Co) compounds, comprised of two layered components, provide exceptionally high capacities (>200 mAh g^{-1}) when used as electrodes in high voltage (4.5–3.0 V) lithium-ion cells; in this respect, they outperform conventional layered $LiCoO_2$, spinel $LiMn_2O_4$ and olivine $LiFePO_4$ electrodes. The structures of these compounds are highly complex; they are characterized by Mn and M cation disorder between the Li_2MnO_3 and $LiMO_2$ components, the disorder being more pronounced when cobalt is introduced into the structure. The Li_2MnO_3 component performs a vital function in the electrochemical operation of $xLi_2MnO_3\cdot(1-x)LiMO_2$ electrodes: 1) the ability to activate the Li_2MnO_3 component by extracting Li_2O in a controlled manner, either chemically or electrochemically, to form a MnO_2 component within a charged electrode structure, makes these materials extremely versatile for tailoring and optimizing their compositional, structural and electrochemical properties; 2) any unactivated Li_2MnO_3 in the composite structure will act as a reservoir for excess lithium that can diffuse from the transitional metal layers into the adjacent lithium-depleted layers during charge to stabilize the electrode structure, thereby enabling the access of high practical capacities; 3) the Li_2MnO_3 units not only serve to stabilize the capacity generating $LiMO_2$ regions of the electrode, but also act as solid electrolyte constituents to facilitate Li^+-ion transport through the structure. The stability of these complex lithium metal oxide electrodes can be enhanced by fluorinating the electrode particles prior to cell assembly to provide robust surface layers. These attributes, therefore, hold considerable promise for further improvements in the compositional design and performance of Li_2MnO_3-stabilized $LiMO_2$ (M = Mn, Ni, Co) electrodes for lithium-ion batteries.

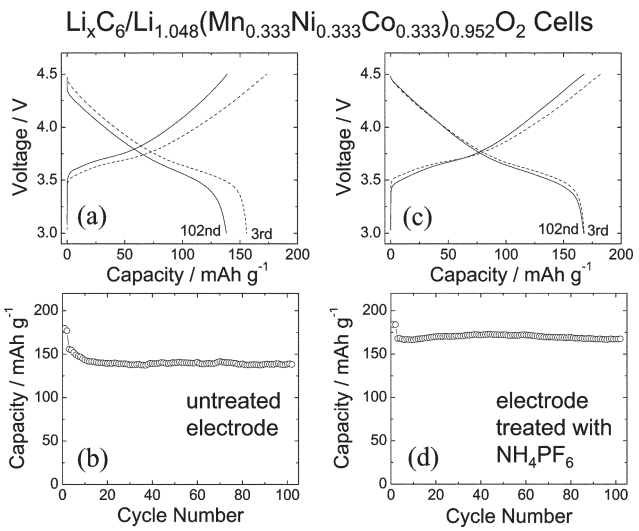

Fig. 12 Charge/discharge voltage profiles for the 3rd and 102nd cycles and capacity *vs.* cycle number plots of lithium full cells (Li_xC_6 anode) with, (a) and (b), an untreated $Li_{1.048}(Mn_{0.33}Ni_{0.33}Co_{0.33})_{0.952}O_2$ electrode and, (c) and (d), an electrode preconditioned with a 2.4×10^{-3} M NH_4PF_6 solution (pH $\approx$ 6.5) prior to cell assembly, respectively.

Acknowledgements

Financial support from the Office of FreedomCar and Vehicle Technologies of the U.S. Department of Energy is gratefully acknowledged.

The submitted manuscript has been created by UChicago Argonne, LLC, Operator of Argonne National Laboratory ("Argonne"). Argonne, a U.S. Department of Energy Office of Science laboratory, is operated under Contract No. DE-AC02-06CH11357. The U.S. Government retains for itself, and others acting on its behalf, a paid-up nonexclusive, irrevocable worldwide license in said article to reproduce, prepare derivative works, distribute copies to the public, and perform publicly and display publicly, by or on behalf of the Government.

References

1 D. Linden and T. B. Reddy, *Handbook of Batteries – 3rd Edition*, McGraw Hill, New York, 2002.
2 S. Basu, *US Pat.*, 4423125, 1983.
3 R. Yazami and Ph. Touzain, *J. Power Sources*, 1983, **9**, 365.
4 K. Mizushima, P. C. Jones, P. J. Wiseman and J. B. Goodenough, *Mater. Res. Bull.*, 1980, **15**, 783.
5 C. H. Chen, J. Liu, M. E. Stoll, G. Henriksen, D. R. Vissers and K. Amine, *J. Power Sources*, 2004, **128**, 278.
6 M. M. Thackeray, P. J. Johnson, L. A. de Picciotto, P. G. Bruce and J. B. Goodenough, *Mater. Res. Bull.*, 1984, **19**, 179.
7 T. Ohzuku, M. Kitagawa and T. Hirai, *J. Electrochem. Soc.*, 1990, **137**, 769.
8 R. J. Gummow, A. de Kock and M. M. Thackeray, *Solid State Ionics*, 1994, **69**, 59.
9 A. K. Pahdi, K. S. Najundaswamy and J. B. Goodenough, *J. Electrochem. Soc.*, 1997, **144**, 1188.
10 A. Yamada, M. Hosoya, S. C. Chunng, Y. Kudo, K. Hinokuma, K. Y. Liu and Y. Nishi, *J. Power Sources*, 2003, **119**, 232.

11 I. Belharouak, W. Lu, D. R. Vissers and K. Amine, *Electrochem. Commun.*, 2006, **8**, 329.
12 G. G. Amatucci, C. N. Schmutz, A. Blyr, C. Sigala, A. S. Gozdz, D. Larcher and J. M. Tarascon, *J. Power Sources*, 1997, **69**, 11.
13 G. G. Amatucci, N. Pereira, T. Zheng and J. M. Tarascon, *J. Electrochem. Soc.*, 2001, **148**, A171.
14 W. Choi and A. Manthiram, *Electrochem. Solid-State Lett.*, 2006, **9**, A245.
15 H. S. Shin, S. H. Park, C. S. Yoon and Y. K. Sun, *Electrochem. Solid-State Lett.*, 2005, **8**, A559.
16 S. H. Kang and K. Amine, *J. Power Sources*, 2005, **146**, 654.
17 M. M. Thackeray, *Prog. Solid State Chem.*, 1997, **25**, 1.
18 M. H. Rossouw and M. M. Thackeray, *US Pat.*, 5166012, 1992.
19 C. S. Johnson, D. W. Dees, M. F. Mansuetto, M. M. Thackeray, D. R. Vissers, D. Argyriou, C.-K. Loong and L. Christensen, *J. Power Sources*, 1997, **68**, 570.
20 R. Collongues, J. Théry and J. P. Boilot, in *Solid Electrolytes, General Principles, Characterization, Materials, Applications*, ed. P. Hagenmuller and W. van Gool, Academic Press, New York, 1978, p. 253.
21 J. T. Kummer, *Prog. Solid State Chem.*, 1972, **7**, 141.
22 M. M. Thackeray and J. Coetzer, *Acta Crystallogr., Sect. B*, 1978, **34**, 71.
23 M. M. Thackeray and J. Coetzer, *Electrochim. Acta*, 1979, **34**, 495.
24 P. G. Bruce, A. R. Armstrong and G. L. Gitzendanner, *J. Mater. Chem.*, 1998, **9**, 193.
25 M. S. Whittingham and P. Y. Zavalij, *Solid State Ionics*, 2000, **131**, 109.
26 M. M. Thackeray, M. H. Rossouw, A. de Kock, A. P. de la Harpe, R. J. Gummow, K. Pearce and D. C. Liles, *J. Power Sources*, 1993, **43–44**, 289.
27 M. H. Rossouw and M. M. Thackeray, *Mater. Res. Bull.*, 1991, **26**, 463.
28 C. S. Johnson, S. D. Korte, J. T. Vaughey, M. M. Thackeray, T. E. Bofinger, Y. Shao-Horn and S. A. Hackney, *J. Power Sources*, 1999, **81–82**, 491.
29 M. H. Rossouw, D. C. Liles and M. M. Thackeray, *J. Solid State Chem.*, 1993, **104**, 464.
30 M. H. Rossouw, A. de Kock, L. A. de Picciotto, M. M. Thackeray, W. I. F. David and R. M. Ibberson, *Mater. Res. Bull.*, 1990, **25**, 173.
31 J.-S. Kim, C. S. Johnson and M. M. Thackeray, *Electrochem. Commun.*, 2002, **4**, 205.
32 J.-S. Kim, C. S. Johnson, J. T. Vaughey, M. M. Thackeray, S. A. Hackney, W. Yoon and C. P. Grey, *Chem. Mater.*, 2004, **16**, 1996.
33 M. M. Thackeray, C. S. Johnson, J. T. Vaughey, N. Li and S. A. Hackney, *J. Mater. Chem.*, 2005, **15**, 2257.
34 C. S. Johnson, N. Li, J. T. Vaughey, S. A. Hackney and M. M. Thackeray, *Electrochem. Commun.*, 2005, **7**, 528.
35 S.-H. Park, S.-H. Kang, C. S. Johnson, K. Amine and M. M. Thackeray, *Electrochem. Commun.*, 2006, **9**, 262.
36 P. Strobel and B. Lambert-Andron, *J. Solid State Chem.*, 1988, **75**, 90.
37 P. G. Bruce and A. R. Armstrong, *Nature*, 1996, **381**, 499–500.
38 W. D. Johnston, R. R. Heikes and D. Sestrich, *J. Phys. Chem. Solids*, 1958, **7**, 1.
39 L. D. Dyer, B. S. Borie and G. P. Smith, *J. Am. Chem. Soc.*, 1954, **76**, 1499.
40 M. M. Thackeray, S.-H. Kang, C. S. Johnson, J. T. Vaughey and S. A. Hackney, *Electrochem. Commun.*, 2006, **8**, 1531.
41 Y. Shao-Horn, S. A. Hackney and B. C. Cornilsen, *J. Electrochem. Soc.*, 1997, **144**, 3147.
42 X. Q. Song, J. F. Ma and R. F. Chen, *J. Inorg. Mater.*, 2000, **15**, 33.
43 B. Ammundsen, J. Paulsen, I. Davidson, R.-S. Liu, C.-H. Shen, J.-M. Chen, L.-Y. Yang and J.-F. Lee, *J. Electrochem. Soc.*, 2002, **149**, A431.
44 K. Numata and S. Yamanaka, *Solid State Ionics*, 1999, **118**, 117.
45 Z. Lu and J. R. Dahn, *J. Electrochem. Soc.*, 2002, **149**, A778.
46 C. P. Grey, W.-S. Yoon, J. Reed and G. Ceder, *Electrochem. Solid-State Lett.*, 2004, **7**, A290.
47 K. Kang and G. Ceder, *Phys. Rev. B*, 2006, **74**, 094105.
48 M. M. Thackeray, W. I. F. David, P. G. Bruce and J. B. Goodenough, *Mater. Res. Bull.*, 1983, **18**, 461.
49 K. Shizuka, T. Kobayashi, K. Okahara, K. Okamoto, S. Kanzaki and R. Kanno, *J. Power Sources*, 2005, **146**, 589.
50 A. Rougier, P. Gravereau and C. Delmas, *J. Electrochem. Soc.*, 1996, **143**, 1168.
51 A. R. Armstrong, M. Holzhapfel, P. Novak, C. S. Johnson, S.-H. Kang, M. M. Thackeray and P. G. Bruce, *J. Am. Chem. Soc.*, 2006, **128**, 8694.
52 C. S. Johnson, J.-S. Kim, C. Lefief, N. Li, J. T. Vaughey and M. M. Thackeray, *Electrochem. Commun.*, 2004, **6**, 1085.
53 Y. Shao Horn, Understanding Phase Transformations in Lithium Battery Materials by Transmission Electron Microscopy, in *Science and Technology of Lithium Batteries*, ed. G. A. Nazri and G. Pistoia, Kluwer Academic Publishers, Dordrecht, 2003, p. 478.
54 C. P. Grey and N. Dupré, *Chem. Rev.*, 2004, **104**, 4493.
55 J. Breger, M. Jiang, N. Dupré, Y. S. Meng, Y. Shao-Horn, G. Ceder and C. P. Grey, *J. Solid State Chem.*, 2005, **178**, 2575.
56 A. Van der Ven and G. Ceder, *Electrochem. Commun.*, 2004, **6**, 1045.
57 K. S. Kang, Y. S. Meng, J. Breger, C. P. Grey and G. Ceder, *Science*, 2006, **311**, 977.
58 W.-S. Yoon, M. Balasubramanian, X.-Q. Yang, Z. Fu, D. A. Fischer and J. McBreen, *J. Electrochem. Soc.*, 2004, **151**, A246.
59 W.-S. Yoon, S. Iannopolis, C. P. Grey, D. Carlier, J. Gorman, J. Reed and G. Ceder, *Electrochem. Solid-State Lett.*, 2004, **7**, A167.
60 Y. S. Meng, G. Ceder, C. P. Grey, W.-S. Yoon, M. Jiang, J. Breger and Y. Shao-Horn, *Chem. Mater.*, 2005, **17**, 2386.
61 Z. Lu, Z. Chen and J. R. Dahn, *Chem. Mater.*, 2003, **15**, 3214.
62 A. Deb, U. Bergmann, S. P. Cramer and E. J. Cairns, *J. Appl. Phys.*, 2005, **97**, 113523.
63 W. Lu, I. Belharouak, D. R. Vissers and K. Amine, *J. Electrochem. Soc.*, 2004, **151**, A246.
64 I. Belharouak, Z. Chen, S.-H. Park and K. Amine, to be published.
65 C. S. Johnson, N. Li, C. Lefief and M. M. Thackeray, *Electrochem. Commun.*, 2007, **9**, 787.
66 Y. Wu and A. Manthiram, *Electrochem. Solid-State Lett.*, 2006, **9**, A221.
67 S.-H. Kang and K. Amine, *J. Power Sources*, 2005, **146**, 654.
68 J-S. Kim, C. S. Johnson, J. T. Vaughey and M. M. Thackeray, *J. Power Sources*, 2006, **153**, 258.
69 S.-H. Kang, C. S. Johnson, J. T. Vaughey, K. Amine and M. M. Thackeray, *J. Electrochem. Soc.*, 2006, **153**, A1186.
70 H. Yang, G. V. Zhuang and P. N. Ross, *J. Power Sources*, 2006, **161**, 573.
71 J. C. Hunter, *J. Solid State Chem.*, 1981, **39**, 142.
72 A. Du Pasquier, A. Blyr, P. Courjal, D. Larcher, G. Amatucci, B. Gerand and J. M. Tarascon, *J. Electrochem. Soc.*, 1999, **146**, 428.
73 Y. Paik, C. P. Grey, C. S. Johnson, J.-S. Kim and M. M. Thackeray, *Chem. Mater.*, 2002, **14**, 5109.
74 W. P. Tang, H. F. Kanoh, X. J. Yang and K. Ooi, *Chem. Mater.*, 2000, **12**, 3271.
75 R. Benedek and M. M. Thackeray, *Electrochem. Solid-State Lett.*, 2006, **9**, A265.
76 Y. Kanai, X. Wang, A. Selloni and R. Car, *J. Chem. Phys.*, 2006, **125**, 234104.
77 R. Gupta and A. Manthiram, *J. Solid State Chem.*, 1996, **121**, 483.
78 G. Kresse and J. Furthmueller, *Comput. Mater. Sci.*, 1996, **6**, 15.
79 G. Kresse and J. Furthmueller, *Phys. Rev. B*, 1996, **54**, 11169.
80 G. Kresse and D. Joubert, *Phys. Rev. B*, 1999, **59**, 1758.
81 Y. Marcus, *J. Chem. Soc., Faraday Trans.*, 1991, **87**, 2995.
82 A. van de Walle, personal communication.
83 R. Chitrakar, H. Kanoh, Y. Miyai and K. Ooi, *Ind. Eng. Chem. Res.*, 2001, **40**, 2054.
84 R. Benedek and M. M. Thackeray, unpublished calculations.
85 H.-W. Chan, J.-G. Duh and S.-R. Sheen, *Surf. Coat. Technol.*, 2004, **118–189**, 116.

86 J. Cho, Y. J. Kim, T.-J. Kim and B. Park, *Angew. Chem., Int. Ed.*, 2001, **40**, 18.
87 D. Ahn, J. G. Lee, J. S. Lee, J. Kim, J. Cho and B. Park, *Curr. Appl. Phys.*, 2007, **7**, 172.
88 M. M. Thackeray, C. S. Johnson, J.-S. Kim, K. C. Lauzze, J. T. Vaughey, N. Dietz, D. Abraham, S. A. Hackney, W. Zeltner and M. A. Anderson, *Electrochem. Commun.*, 2003, **5**, 752.
89 J.-S. Kim, C. S. Johnson, J. T. Vaughey, S. A. Hackney, K. A. Walz, W. Zeltner, M. A. Anderson and M. M. Thackeray, *J. Electrochem. Soc.*, 2004, **151**, A1755.
90 W. Choi and A. Manthiram, *Electrochem. Solid-State Lett.*, 2006, **9**, A245.
91 Y.-K. Sun, S.-W. Cho, S.-W. Lee, C. S. Yoon and K. Amine, *J. Electrochem. Soc.*, 2007, **154**, A168.
92 S.-H. Kang and M. M. Thackeray, to be published.